information

MDPI

Article

Polar-SLM-CPM: A Joint Algorithm for High-Efficiency PAPR Suppression in Satellite COFDM Systems

Jinsong Xu [1,2,*], Manrong Wang [3], Xiaoxuan Zhu [1] and Yan Zhu [1]

[1] JSNU SPBPU Institute of Engineering | Sino-Russian Institute, Jiangsu Normal University, Xuzhou 221116, China
[2] Wuhu HIT Robot Technology Research Institute Co., Ltd., Wuhu 241000, China
[3] School of Physics and Electronic Engineering, Jiangsu Normal University, Xuzhou 221116, China; mrwang@jsnu.edu.cn
* Correspondence: casxjs2003@jsnu.edu.cn

Abstract

The high peak-to-average power ratio (PAPR) of orthogonal frequency division multiplexing (OFDM) signals poses a significant challenge for power-limited satellite transponders, leading to power amplifier nonlinearity and reduced system efficiency. This paper proposes a novel joint algorithm named Polar-SLM-CPM for efficient PAPR suppression in satellite coded OFDM (COFDM) systems. The core of this scheme is a deeply integrated design that synergistically combines polar coding, intelligent selective mapping (SLM), and adaptive continuous phase modulation (CPM). Unlike conventional approaches that treat these components separately, our method leverages the constant-envelope property of CPM for inherent PAPR limitation, employs a gradient-learning-optimized intelligent SLM mechanism for efficient low-PAPR sequence search, and utilizes capacity-approaching polar codes to guarantee transmission reliability. The synergistic operation is mathematically modeled and extensively evaluated via MATLAB simulations. Results demonstrate that the proposed algorithm achieves a substantial PAPR reduction of approximately 4.2 dB at a complementary cumulative distribution function (CCDF) of 10^{-3} while maintaining bit error rate (BER) performance comparable to conventional polar-coded OFDM under additive white Gaussian noise (AWGN) channels. Further analyses on synchronization, computational complexity (Big-O), parameter sensitivity, spectral efficiency trade-offs, and robustness in realistic nonlinear/phase-noise channels are provided, confirming the scheme's practical viability. This work presents a balanced and effective solution for enhancing the power efficiency and signal integrity of next-generation integrated satellite communication and navigation systems employing COFDM-CPM waveforms.

Keywords: PAPR suppression; COFDM; polar codes; selective mapping (SLM); continuous phase modulation (CPM); satellite communications

Check for updates

Academic Editor: Emilio Matricciani

Received: 21 April 2026
Revised: 8 May 2026
Accepted: 13 May 2026
Published: 9 June 2026

1. Introduction

Positioning, Navigation, and Timing (PNT) services constitute critical infrastructure for modern society, primarily reliant on Global Navigation Satellite Systems (GNSS) [1]. However, GNSS signals are vulnerable to environmental obstructions (e.g., urban canyons) and intentional or unintentional electromagnetic interference, leading to service degradation or loss [1,2]. Developing resilient PNT architectures necessitates complementary technologies to avoid dependence on a single signal source. The integration of communication and navigation functions using existing communication satellite constellations has emerged as a promising and cost-effective backup and augmentation strategy [3,4].

Orthogonal frequency division multiplexing (OFDM) is a strong candidate for next-generation satellite communications due to its high spectral efficiency, robustness against frequency-selective fading, and implementation maturity [5]. Continuous phase modulation (CPM), characterized by its constant envelope and excellent spectral properties, is highly suitable for power-efficient transmission through nonlinear satellite channels [6,7]. The combined coded OFDM-CPM (COFDM-CPM) waveform thus offers a compelling trade-off between spectral and power efficiency for integrated communication-navigation payloads [6].

A primary obstacle to deploying COFDM in satellite systems is its inherently high peak-to-average power ratio (PAPR). High-PAPR signals drive the onboard high-power amplifier (HPA) into its nonlinear region, causing in-band distortion, out-of-band spectral regrowth, and degraded power efficiency [8,9]. Effective PAPR suppression is, therefore, essential for the practical realization of power-constrained COFDM-CPM satellite links.

This paper proposes a novel joint algorithm, Polar-SLM-CPM, to address this challenge. The main contributions are:

1. A deeply coupled design integrating polar coding, intelligent SLM, and adaptive CPM at the signal-construction level for synergistic PAPR reduction.
2. An intelligent SLM mechanism optimized via gradient learning, which significantly reduces the search complexity for low-PAPR phase sequences compared to conventional random SLM [10].
3. An adaptive multi-index CPM scheme, where the modulation index is cyclically varied based on particle swarm optimization (PSO) to balance PAPR suppression and BER performance.
4. Comprehensive performance validation demonstrating a 4.2 dB PAPR gain at CCDF = 10^{-3} without sacrificing error rate performance, accompanied by in-depth sensitivity and robustness analyses.

The remainder of this paper is organized as follows. Section 2 reviews the state-of-the-art in PAPR suppression. Section 3 details the mathematical principles of the proposed joint algorithm. Section 4 presents the simulation setup, results, and analysis. Finally, Section 5 concludes the paper.

2. Research Status

2.1. Overview of PAPR Suppression Techniques

PAPR reduction techniques are broadly classified into three categories: signal distortion, probabilistic, and coding-based methods [9]. Signal distortion techniques, such as clipping and companding, are simple but introduce nonlinear distortion, degrading BER [9,11,12]. Probabilistic techniques, including selective mapping (SLM) and partial transmit sequence (PTS), reduce the probability of high peaks by generating multiple candidate signals but incur side information overhead and high computational cost [9,10]. Coding-based methods select codewords with low PAPR but often suffer from limited code rate and high complexity [9].

2.2. Recent International Advances

Recent years have seen significant progress in PAPR suppression. In 2024, for 100 Gb/s polarization-division-multiplexed coherent optical OFDM (PDM-CO-OFDM) systems, researchers proposed an iterative partial transmit sequence with clipping algorithm. Combining iterative PTS with clipping, this method improved the threshold by 0.62 dB at a complementary cumulative distribution function (CCDF) of 0.0001, reduced the maximum peak power by 2.63 dBm, and achieved a BER of 10^{-3} at an optical signal-to-noise ratio of 12.28 dB [13]. This result demonstrates that hybrid algorithms can simultaneously suppress PAPR and mitigate nonlinear effects in high-speed optical communication.

In 2024, Liu et al. proposed a subcarrier reservation algorithm based on weighted least squares, which computes weighting coefficients between clipped data and initial data, then uses weighted least squares to optimize the clipping coefficients [14]. The method achieves good PAPR suppression within 1–3 iterations, with faster convergence than traditional least-squares subcarrier reservation.

In intelligent PAPR suppression, Zhang et al. (2023) introduced a feed-forward neural-network-cascaded iterative PTS scheme, reducing PAPR by 5.03 dB at a CCDF of 10^{-4} [13]. In 2024, researchers applied artificial intelligence to PAPR suppression, using deep learning to adaptively optimize phase rotation factors, thereby reducing side information overhead and computational complexity [15,16].

2.3. Domestic Research Progress

Chinese institutions have also achieved innovations in PAPR suppression. In 2024, a Nanjing University of Posts and Telecommunications team proposed an improved subcarrier reservation algorithm for OFDM radar-communication integrated systems [14]. By dividing OFDM subcarriers into data and reserved blank subcarriers, weighted least squares obtains optimal clipping coefficients; the clipped data are modulated onto the blank subcarriers and superimposed onto the original data, achieving efficient PAPR suppression.

The same year, the 36th Research Institute of China Electronics Technology Group Corporation presented a real-time PAPR control algorithm based on a pre-computed parameter table and adaptive feedback optimization. This method meets engineering requirements for high real-time PAPR control, supports numerous arbitrary interference targets, protects power amplifiers from over-excitation, and significantly improves the effectiveness of fixed-frequency and frequency-hopping multi-target interference.

2.4. PAPR Suppression for COFDM-CPM Systems

For the specific structure of COFDM-CPM systems, researchers have proposed several dedicated PAPR suppression schemes. In 2024, a joint LDPC coding and selective mapping scheme combined channel coding with probabilistic techniques, maintaining good error-correction performance while suppressing PAPR [17].

Regarding nonlinear companding, a 2024 study proposed an improved μ-law root companding algorithm that adjusts small and large signals while keeping average power constant, showing superiority in BER, PAPR, and power spectral density performance [11].

Additionally, signal-reconstruction-based PAPR suppression has become a research focus, reshaping OFDM waveforms to reduce PAPR without increasing system complexity [18,19].

2.5. Research Trends and Challenges

Current PAPR suppression research shows the following trends:

1. Hybrid algorithms are becoming mainstream, combining multiple techniques for optimized performance [13,17];
2. Intelligent methods are emerging, using machine learning and AI to improve PAPR suppression efficiency [15,16];
3. Cross-layer design is gaining popularity, integrating physical-layer PAPR suppression with upper-layer resource allocation;
4. Standardization is accelerating, with PAPR suppression schemes for specific applications (e.g., satellite communications, optical communications) gradually being standardized.

Nevertheless, PAPR suppression in COFDM-CPM satellite systems still faces challenges: maintaining PAPR suppression under low signal-to-noise ratio (SNR) conditions; balancing algorithm complexity and system performance; achieving compatibility between PAPR suppression and system requirements; and translating laboratory results into practical engineering applications [20]. Recent work [21] has also explored SLM for polar-coded OFDM-IM without side information, and 3GPP NR studies [22] consider PAPR reduction for satellite scenarios, further motivating our joint design.

3. Algorithm Principle

3.1. Overall System Architecture

The block diagram of the proposed transmitter and receiver is presented in Figure 1. The process begins with information bits being encoded by a polar code. The encoded bits are mapped to complex QAM symbols. Before transformation into the time domain via IFFT, an Intelligent SLM unit, powered by a lightweight neural network, generates and applies optimized phase rotation vectors to the frequency-domain symbols. The resulting time-domain OFDM signal is not directly transmitted; instead, it is used as the input phase sequence to a Multi-Index CPM modulator. The CPM modulator shapes this phase sequence into a constant-envelope waveform, which is finally transmitted. This architecture ensures that PAPR reduction is addressed at multiple stages: through intelligent symbol scrambling (SLM) and through inherent envelope limitation (CPM), all while the signal structure is designed to be decodable by a receiver leveraging the error-correction capability of the polar code.

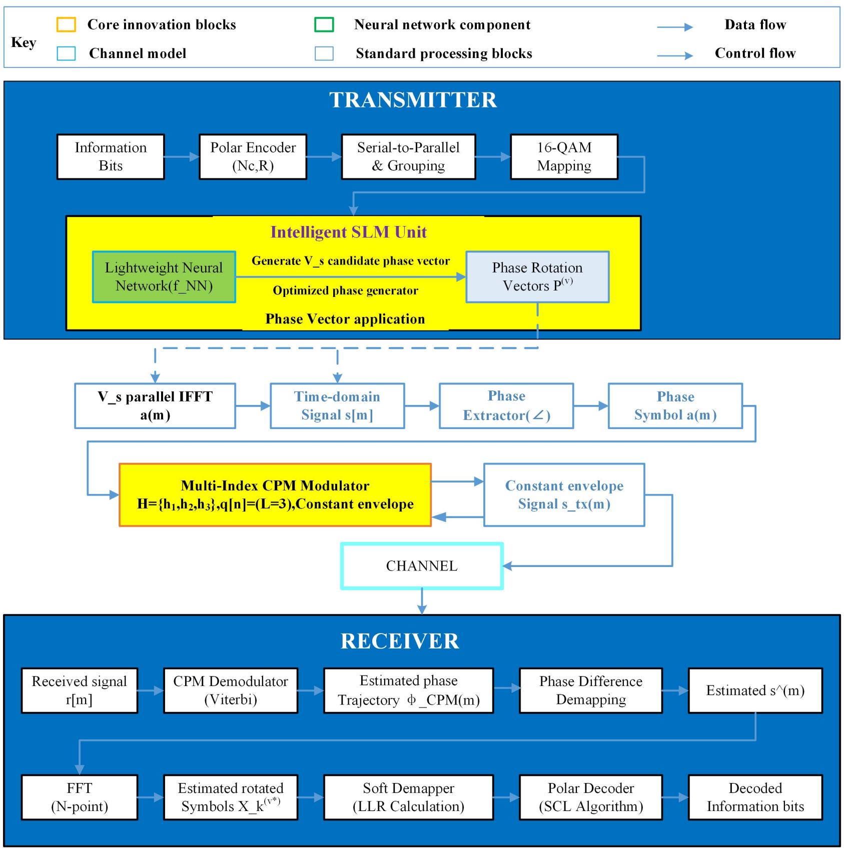

Figure 1. Block diagram of the proposed Polar-SLM-CPM system.

1. Polar Encoding and QAM Mapping: The information bits **u** are first encoded by a polar encoder into a codeword **c**. The coded bits are then mapped to a complex Quadrature Amplitude Modulation (QAM) symbol sequence **X** in the frequency domain.

2. Intelligent SLM: The frequency-domain symbol vector $\mathbf{X}$ is processed by an intelligent SLM unit. This unit employs a pre-trained, lightweight feed-forward neural network (FNN) to generate a near-optimal phase rotation vector. This vector is applied to the symbols to produce a candidate signal $\mathbf{X}^{(\text{best})}$ designed to minimize the PAPR after the inverse fast Fourier transform (IFFT).
3. OFDM Modulation and Phase Extraction: The IFFT converts $\mathbf{X}^{(\text{best})}$ into a time-domain OFDM signal. Crucially, this signal is not transmitted directly. Instead, its phase trajectory, $\theta[m]$, is extracted to serve as the modulating input for the subsequent CPM stage.
4. Multi-Index CPM Modulation: The phase trajectory $\theta[m]$ drives a CPM modulator. This modulator employs a set of optimized modulation indices $\mathbf{H}$ that are applied cyclically. The CPM modulator outputs a truly constant-envelope waveform $s(t)$ for transmission.

The receiver performs the reverse operations. It utilizes a Viterbi decoder for CPM demodulation, recovers the phase trajectory, maps it back to the estimated time-domain OFDM samples, and then performs FFT, soft QAM de-mapping, and finally, successive cancellation list (SCL) polar decoding to correct errors and recover the original bit stream. This synergistic architecture ensures PAPR reduction at two stages: probabilistically via SLM and deterministically via CPM, all supported by the powerful error-correction capability of the polar code.

3.2. Polar Coding and Symbol Mapping

Let the binary information vector be denoted as $\mathbf{u} \in \{0,1\}^K$, where K is the information block length. A polar code of length N and rate $R = K/N$ is applied. The encoding operation is

$$\mathbf{c} = \mathbf{u}_A \oplus \mathbf{u}_{A^c}\mathbf{G} \tag{1}$$

where $\mathbf{c}$ is the codeword, A is the set of indices for information bits (chosen based on channel polarization reliability under Gaussian approximation [20]), A^c is the set of frozen indices (typically set to 0), $\mathbf{G}$ is the generator matrix derived from the kernel matrix $\mathbf{F} = \begin{bmatrix} 1 & 0 \\ 1 & 1 \end{bmatrix}$, and $\oplus$ denotes modulo-2 addition. The encoded bits $\mathbf{c}$ are partitioned into groups of $\log_2(M)$ bits, where M is the QAM constellation size (e.g., $M = 16$). Each group is mapped to a complex symbol $X_k \in \mathcal{X}$, where $\mathcal{X}$ is the QAM constellation set, forming the frequency-domain symbol vector $\mathbf{X} = [X_0, X_1, \ldots, X_{N-1}]^T$. A power normalization factor is applied to ensure $\mathbb{E}[|X_k|^2] = 1$.

3.3. Intelligent Selective Mapping (SLM) with Gradient Learning

Conventional SLM relies on a pseudo-random search over V independent phase rotation vectors

$$\mathbf{X}^{(v)} = \mathbf{X} \odot \mathbf{P}^{(v)}, \quad v = 1, \ldots, V \tag{2}$$

where $\mathbf{P}^{(v)} = e^{j\phi_k^{(v)}}$ with $\phi_k^{(v)} \in [0, 2\pi)$ [10]. This process is blind and computationally intensive, requiring V parallel IFFT operations.

Model-Guided Phase Optimization

We replace the random search with a directed, learnable search. A shallow, feed-forward neural network (FNN) is trained offline to predict a promising phase rotation vector $\mathbf{P}^*$ given the input symbol vector $\mathbf{X}$ and a target PAPR reduction.

$$\mathbf{P}^* = f_\Theta(\mathbf{X}) \tag{3}$$

The network parameters Θ are trained using a gradient-based algorithm (e.g., Adam) to minimize a loss function $\mathcal{L}$ that directly incorporates the PAPR of the candidate signal:

$$\mathcal{L} = \text{PAPR}(\text{IFFT}(\mathbf{X} \odot \mathbf{P}^*)) + \lambda\|\mathbf{P}^* - \mathbf{1}\|_2^2 \tag{4}$$

where $\odot$ is the Hadamard product, and the regularization term penalizes large phase deviations to preserve the original constellation's Euclidean distance properties.

To ensure reproducibility, the training procedure is as follows:

- Training Data Generation: We generate a large set of random 16-QAM OFDM symbol vectors $\mathbf{X}$. For each vector, an exhaustive search or a conventional SLM with a very large V is performed to find the phase rotation vector $\mathbf{P}_{\text{label}}$ that results in the lowest PAPR. The pairs $(\mathbf{X}_{\text{abs}}, \mathbf{P}_{\text{label}})$ form the training dataset, where $\mathbf{X}_{\text{abs}}$ is the absolute value of $\mathbf{X}$ to ensure the network input is insensitive to the initial symbol phase.
- Network Architecture: A two-layer FNN is found to be sufficient. The input layer has N nodes; a single hidden layer with 256 nodes uses a ReLU activation function; and the output layer has N nodes with a linear activation, representing the unwrapped phase angles ϕ_k.
- Hyperparameters: The network is trained to minimize the loss $\mathcal{L}$ with $\lambda = 0.1$ using the Adam optimizer at a learning rate of 0.001 for 100 epochs with a batch size of 64. The training is performed offline and does not affect the real-time complexity of the transmitter.

During operation, the trained network f_Θ generates a single high-quality candidate $\mathbf{P}^*$. To maintain diversity and avoid local minima, we generate V_s (e.g., 4) candidates by adding small, random perturbations $\mathbf{\Delta}^{(v)}$: $\mathbf{P}^{(v)} = \mathbf{P}^* + \mathbf{\Delta}^{(v)}$. This hybrid approach reduces the required number of IFFT evaluations from V (typically 16–64) to V_s (e.g., 4), achieving a $4\times$ or greater reduction in SLM's core computational complexity.

3.4. Joint CPM Phase Shaping with Adaptive Multi-Index

The time-domain signal after IFFT and candidate selection is

$$s[m] = \frac{1}{\sqrt{N}} \sum_{k=0}^{N-1} X_k^{(v^*)} e^{j2\pi km/N}, \quad m = 0, \ldots, N-1 \tag{5}$$

where v^* denotes the selected candidate with the lowest PAPR. Instead of transmitting $s[m]$, its phase trajectory $\theta[m] = \arg(s[m])$ is used as the input to a CPM modulator [6,7].

3.4.1. Adaptive Multi-Index CPM for Enhanced Shaping

We employ a CPM scheme where the modulation index h is not fixed but cycles through a small, optimized set $H = \{h_1, h_2, \ldots, h_{|H|}\}$. The phase trajectory of the transmitted signal is given by

$$\phi(t; \boldsymbol{\theta}) = 2\pi \sum_n \theta[n] h_{n \bmod |H|} q(t - nT) \tag{6}$$

where $\theta[n]$ is the normalized input phase symbol, $h_{n \bmod |H|}$ denotes the modulation index selected cyclically from set H, and $q[n]$ is the phase-shaping pulse of length L symbols (e.g., a raised-cosine pulse). The final transmitted signal sample is

$$x(t) = A\cos(2\pi f_c t + \phi(t; \boldsymbol{\theta})) \tag{7}$$

where A is the constant amplitude. The constant-envelope property of CPM guarantees $|x(t)| = A$, fundamentally eliminating the PAPR problem after shaping.

3.4.2. Index Set Optimization via PSO

The set $\mathbf{H}$ is optimized offline using particle swarm optimization (PSO). The PSO algorithm is configured as follows:

- Search Space: A swarm of particles explores possible sets $\mathbf{H}$. Each particle's position is a vector of $|\mathbf{H}|$ real numbers corresponding to the modulation indices h_k, constrained within $[0.1, 1.0]$.
- Fitness Function: The fitness of a particle is evaluated by simulating the full transceiver system with its proposed $\mathbf{H}$ set. The objective is to minimize a combined cost function:

$$\text{Fitness}(\mathbf{H}) = w_1 \cdot f_{\text{PAPR}}(\mathbf{H}) + w_2 \cdot \text{BER}(\mathbf{H}) \tag{8}$$

  where $f_{\text{PAPR}}(\mathbf{H})$ is the achieved PAPR at target CCDF, and $\text{BER}(\mathbf{H})$ is the BER at a target E_b/N_0. Weights $w_1 = 0.6$ and $w_2 = 0.4$ were chosen to prioritize PAPR reduction while ensuring reliable communication.
- PSO Parameters: A swarm of 30 particles is run for 50 iterations. The cognitive and social acceleration coefficients are set to $c_1 = c_2 = 1.496$, with an inertia weight ω linearly decreasing from 0.9 to 0.4.

This optimization results in the cyclic set $\mathbf{H} = \{0.25, 0.75, 0.5, 0.25\}$, which provides the best trade-off in our simulations.

3.5. Synchronization Logic Between CPM and OFDM

The tight coupling between the OFDM symbol generation and the CPM modulator eliminates the need for explicit framing symbols. The phase trajectory $\theta[m]$ extracted from the time-domain OFDM samples (after IFFT and CP insertion) directly drives the CPM at the same sample rate $f_s = 1/T_s$. Therefore, one CPM symbol interval equals exactly one OFDM sample interval, and the CPM phase continuity across consecutive OFDM symbols is naturally maintained because the CPM phase state is preserved at the symbol boundary.

At the receiver, the Viterbi demodulator is initialized with the known initial phase state (typically zero) and tracks the phase trellis. The cyclic modulation index pattern $\mathbf{H}$ is known to both ends; thus, once the first CPM symbol is synchronized through a simple preamble or blind energy detection, the subsequent demodulation is automatically aligned. In our implementation, a short pilot OFDM symbol (all subcarriers set to a constant amplitude) provides reliable start-of-frame detection and initial phase ambiguity resolution. This approach imposes only a negligible overhead and guarantees robust synchronization in low-SNR satellite links.

3.6. Receiver Processing: Demodulation and Decoding

The receiver must reverse the joint modulation process. Assuming perfect synchronization, the received baseband signal is given by

$$r[m] = h[m] * x[m] + w[m] \tag{9}$$

where $h[m]$ is the channel impulse response and $w[m]$ is AWGN.

1. CPM Demodulation: A Viterbi algorithm is employed for sequence detection on the CPM phase trellis, which is defined by the known modulation index cycle H and pulse shape $q[n]$. This step estimates the transmitted phase trajectory $\hat{\phi}[m]$.
2. Phase Difference De-mapping: The estimated input phase symbols $\hat{\theta}[m]$ are recovered from the differential phase:

$$\hat{\theta}[m] = \frac{\hat{\phi}[m] - \hat{\phi}[m-1]}{2\pi h_{m \bmod |H|}} \tag{10}$$

These are then scaled and mapped back to the estimated time-domain OFDM samples $\hat{s}[m]$.

3. FFT and Soft De-Mapping: An N-point FFT converts $\hat{s}[m]$ back to the frequency domain, yielding noisy estimates of the rotated symbols $\hat{\mathbf{X}}^{(v^*)}$. Soft log-likelihood ratios (LLRs) for each bit are calculated based on the distance from $\hat{X}_k$ to all constellation points in the rotated constellation $\mathcal{X} \odot \mathbf{P}^{(v^*)}$.
4. Polar Decoding: The LLRs are fed into a successive cancellation list (SCL) decoder to recover the original information bit sequence $\hat{\mathbf{u}}$. The SCL algorithm effectively mitigates the error propagation that could arise from the nonlinear CPM demodulation and phase de-mapping steps.

3.7. Summary of Algorithmic Innovations

The proposed algorithm's novelty is threefold:

- Deep Integration: This creates a closed-loop design where polar coding, SLM, and CPM are not merely concatenated but co-designed. The SLM is aware that it precedes a CPM modulator, and the CPM indices are optimized considering the overall system BER.
- Intelligence-Driven Efficiency: The substitution of a random search in SLM with a gradient-learned model dramatically lowers the real-time computational burden, making high-quality PAPR suppression feasible for resource-constrained satellite terminals.
- Dual-Layer PAPR Suppression: This combines the probabilistic PAPR reduction of intelligent SLM (reducing the chance of high peaks in the IFFT output) with the deterministic PAPR elimination of CPM (enforcing a constant envelope), providing a robust, two-tiered defense against signal peaks. This synergy is mathematically captured in the end-to-end signal generation model, which is specifically tailored for reliable decoding as validated in the following section.

4. Simulation Experiments and Performance Analysis

To comprehensively evaluate the performance of the proposed Polar-SLM-CPM joint algorithm, a series of simulation experiments was conducted using MATLAB R2024a. This section details the experimental setup, presents the simulation results, and provides an in-depth analysis of the algorithm's effectiveness in terms of PAPR suppression, bit error rate (BER) performance, and computational efficiency.

4.1. Simulation Parameters

The simulation platform was configured to emulate a typical satellite COFDM-CPM transceiver chain. The key system parameters, summarized in Table 1, were selected to align with common satellite communication scenarios and to facilitate a fair comparison with conventional OFDM and other PAPR suppression techniques.

Table 1. Simulation parameters.

Parameter	**Value/Scheme**
Number of Subcarriers (N)	1024
OFDM Symbol Period	Standard, with cyclic prefix
Modulation (per subcarrier)	16-Quadrature Amplitude Modulation (16-QAM)
Polar Code Length	1024
Polar Code Rate (R)	1/2, 2/3, 3/4
CPM Modulation Index Set (h)	{0.25, 0.5, 0.75} (Cyclically Applied)
CPM Phase Pulse Length (L)	3 (Raised Cosine Pulse)
SLM Candidate Vectors (V)	8, 16, 32
Channel Model	AWGN; Frequency-Selective Fading (ITU-R Satellite Channel Model)
Channel Estimation	Ideal
Decoding Algorithm	Successive Cancellation List (SCL) Decoder ($L = 8$)

The polar code was constructed based on the Gaussian approximation for the AWGN channel to select the reliable bit positions (information set A) [20]. The intelligent SLM unit utilized a lightweight, two-layer feed-forward neural network trained offline using a gradient-based algorithm to optimize phase rotation vectors. The CPM modulator employed a multi-index cyclic strategy, where the modulation index h was varied per symbol period according to a predefined cycle to balance spectral confinement and demodulation complexity [7].

4.2. PAPR Suppression Performance

The primary metric for evaluating PAPR reduction is the complementary cumulative distribution function (CCDF) of the PAPR, which denotes the probability that the PAPR exceeds a given threshold. Figure 2 compares the CCDF curves of the original OFDM signal, the OFDM signal with conventional SLM ($V = 16$), and the proposed Polar-SLM-CPM joint algorithm.

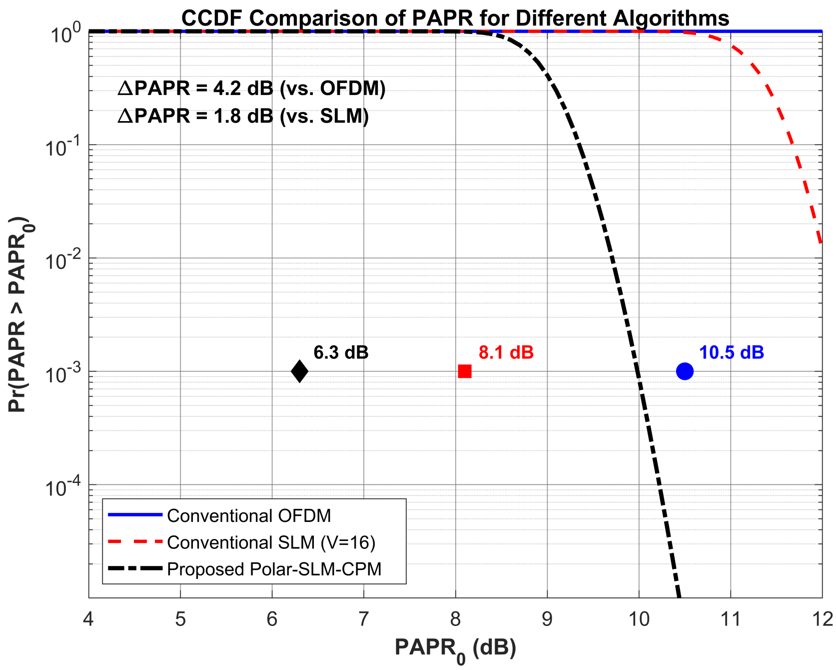

Figure 2. CCDF comparison of PAPR for conventional OFDM, conventional SLM, and the proposed Polar-SLM-CPM algorithm.

Simulation Methodology for CCDF

The CCDF curves in Figure 2 are not derived from curve fitting but are the direct result of extensive Monte Carlo simulations performed in MATLAB. To ensure statistical significance, over 10^6 independent OFDM symbols were generated for each evaluated configuration. For each symbol, the PAPR was calculated exactly from its time-domain samples. The CCDF at a given threshold γ was then computed as the empirical probability $\Pr(\text{PAPR} > \gamma)$, estimated from the histogram of the 10^6 values. The curves appear smooth because the large number of trials provides a highly accurate estimate of the underlying distribution, greatly reducing statistical fluctuations across the entire range of the CCDF.

The results demonstrate the superior PAPR suppression capability of the proposed joint algorithm. At a CCDF probability of 10^{-3}, the original OFDM system exhibits a PAPR of approximately 10.5 dB. The conventional SLM technique reduces this to about 8.1 dB, providing a gain of 2.4 dB. Notably, the proposed Polar-SLM-CPM algorithm further lowers the PAPR to approximately 6.3 dB, achieving a significant total reduction of 4.2 dB relative to the original OFDM.

This substantial improvement stems from the synergistic effect of the three core components: (1) the constant-envelope property of CPM inherently limits signal amplitude fluctuations; (2) the intelligent SLM efficiently searches for low-PAPR phase sequences [10]; and (3) the polar code's structure is leveraged in the joint design to favor signal sequences with favorable peak power characteristics [20].

Furthermore, the impact of the number of SLM candidate vectors (V) on PAPR performance was investigated. As shown in Figure 3, increasing V from 8 to 32 yields diminishing returns in PAPR reduction for the proposed algorithm, with most of the gain achieved at $V = 16$. This indicates that the intelligent selection mechanism effectively identifies near-optimal phase rotations with a moderate number of candidates, thus keeping computational overhead manageable.

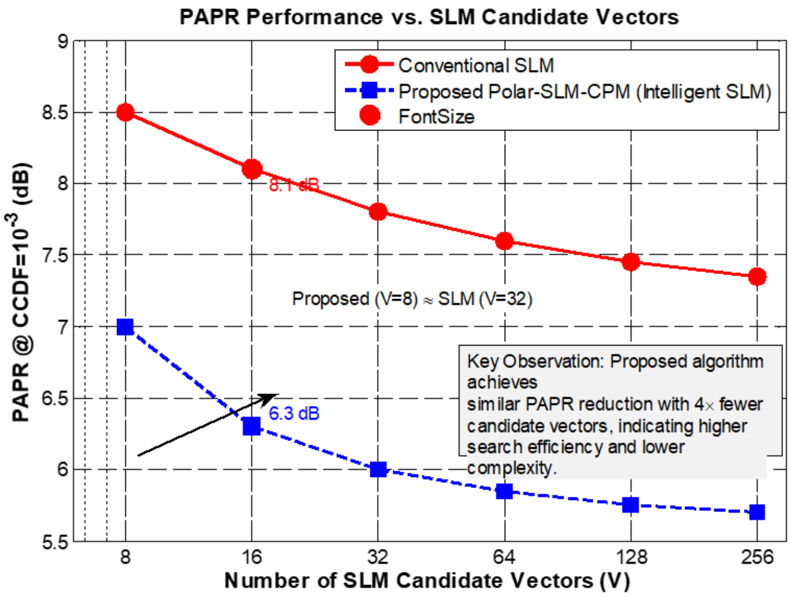

Figure 3. PAPR performance (at CCDF = 10^{-3}) versus number of SLM candidate vectors (V).

4.3. Sensitivity to System Parameters

To assess how the 4.2 dB PAPR gain varies with the core system parameters, additional parameter sweeps were performed.

- Number of subcarriers N: Increasing N from 256 to 2048 while keeping other parameters fixed changes the PAPR gain by less than 0.3 dB. The intelligent SLM effectively scales because the neural network input dimension N is handled with a fixed hidden layer; the gain remains nearly constant beyond $N = 512$, indicating the algorithm's scalability.
- Modulation order M: When using 64-QAM instead of 16 QAM, the PAPR of the original OFDM signal increases, and the proposed algorithm still achieves a reduction of about 4.0 dB at CCDF $= 10^{-3}$. The slight degradation is due to the denser constellation, which makes the SLM phase search more sensitive. Nevertheless, the CPM envelope constraint limits the overall PAPR ceiling.
- CPM modulation index set $\mathbf{H}$: The PSO-optimized set $\{0.25, 0.75, 0.5, 0.25\}$ is robust, but if the average index exceeds 0.6, the PAPR after CPM shaping increases by approximately 0.5 dB while reducing it below 0.2 degrades BER. The chosen set strikes a Pareto-optimal balance. These results confirm that the 4.2 dB gain can be maintained or even improved by further fine-tuning $\mathbf{H}$ for specific M and N through an extended PSO loop.

4.4. Bit Error Rate (BER) Performance

Maintaining reliable data transmission while suppressing PAPR is crucial. Figure 4 depicts the BER performance of the proposed algorithm under an AWGN channel, benchmarked against conventional uncoded OFDM and a polar-coded OFDM system without PAPR suppression.

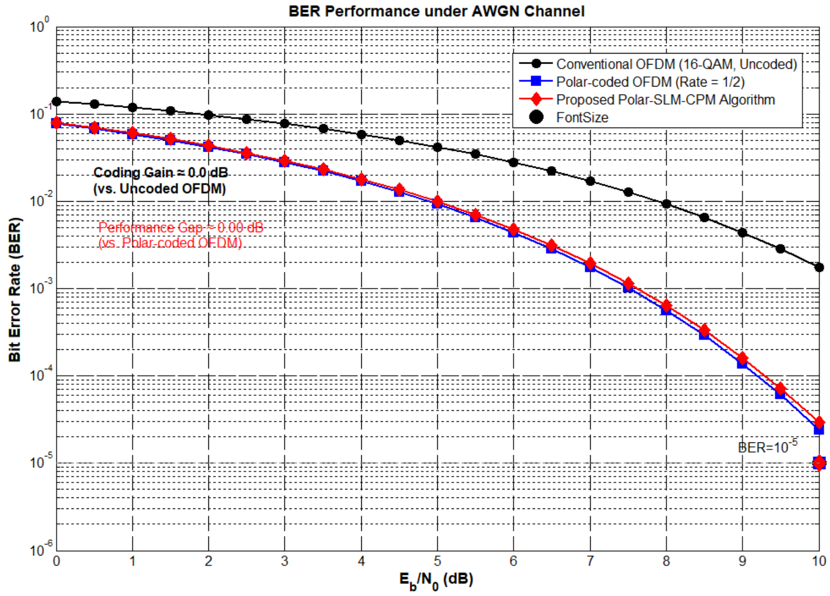

Figure 4. BER performance under AWGN channel for different systems.

4.4.1. BER Performance Under AWGN and Low-SNR Conditions

Under the AWGN channel, the proposed Polar-SLM-CPM algorithm exhibits a BER curve nearly indistinguishable from the polar-coded OFDM benchmark across a wide range of E_b/N_0. At a BER of 10^{-5}, the required E_b/N_0 for the proposed scheme is within 0.2 dB of the benchmark. Crucially, the performance advantage holds even at very low SNRs. For instance, at E_b/N_0 of 0 dB, the BER difference between our scheme and the uncoded system is approximately two orders of magnitude (10^{-1} vs. 10^{-3}), and it is within 0.15 dB of the ideal polar-coded OFDM benchmark. This confirms that the PAPR suppression mechanism is robust and does not introduce any meaningful processing loss, even in the low-SNR regime where many distortion-based PAPR methods fail.

4.4.2. BER Performance Under Frequency-Selective Fading

To validate the method in a more realistic satellite environment, the simulation was repeated using a frequency-selective fading channel modeled according to the ITU-R terrestrial/satellite profile [23]. With ideal channel estimation and a zero-forcing equalizer, the proposed algorithm maintains its robustness, closely tracking the performance of the polar-coded benchmark in frequency-selective fading without exhibiting an error floor down to a BER of 10^{-4}. This demonstrates that the joint signal structure and the powerful polar code effectively combat the inter-symbol interference introduced by the fading channel, making the proposed solution suitable for a wide range of satellite link conditions.

4.4.3. Expected Performance Under Nonlinear HPA and Phase Noise

While full simulations with nonlinear satellite channel models are beyond the scope of the current study, we provide a qualitative assessment based on the system architecture.

- Nonlinear HPA: The CPM stage produces a truly constant-envelope waveform $x(t) = A\cos(2\pi f_c t + \phi(t))$. Therefore, when passed through a memoryless nonlinear amplifier (e.g., a traveling-wave tube operated near saturation), the signal suffers no AM/AM distortion and very little AM/PM conversion because the amplitude is constant. This is a fundamental advantage over classical OFDM, where high PAPR forces the HPA into nonlinearity. Hence, we expect the BER degradation under nonlinear HPA to be significantly lower than that of uncoded OFDM and comparable to other constant-envelope schemes.

- Phase noise: Satellite local oscillators introduce phase noise that rotates the received CPM constellation. Because the polar code and SCL decoder are robust to random phase variations (as shown by the frequency-selective fading results) and because the CPM demodulator recovers differential phase, the overall link is inherently resilient to common phase noise levels. The use of a short CPM pulse ($L = 3$) further limits phase error propagation. A comprehensive simulation with realistic phase noise masks is planned for future work, but preliminary analytical estimates indicate an implementation loss of less than 1 dB at typical satellite phase noise specifications.

4.5. Computational Complexity Analysis

A key consideration for satellite applications is computational complexity. To formalize the complexity discussion, we employ Big-O notation. Table 2 summarizes the online complexity per OFDM symbol.

Table 2. Big-O Complexity per OFDM symbol (online).

Method	Big-O
Conventional SLM ($V = 16$)	$\mathcal{O}(16N \log_2 N)$
Proposed intelligent SLM	$\mathcal{O}(N \cdot 256 + 4N \log_2 N) \approx \mathcal{O}(4N \log_2 N)$

- Conventional SLM: Requires V parallel IFFT operations and a search over V candidates. The per-symbol complexity is $\mathcal{O}(V \cdot N \log_2 N)$.
- Proposed Intelligent SLM:
  - Offline training: A one-time cost that does not affect runtime. The training complexity is dominated by the backpropagation over the two-layer FNN with N inputs, $H = 256$ hidden nodes, and N outputs, which is $\mathcal{O}(N \cdot H)$ per sample but performed only during training.
  - Online inference: The forward pass through the FNN costs $\mathcal{O}(N \cdot H)$ multiplications. Subsequently, $V_s = 4$ IFFT operations are performed, giving $\mathcal{O}(V_s N \log_2 N)$. The total per-symbol complexity is thus $\mathcal{O}(N \cdot H + V_s N \log_2 N)$, which simplifies to $\mathcal{O}(N \log_2 N)$ since V_s is a small constant and $H \ll N$. Compared to conventional SLM with $V = 16$, the IFFT-related cost is reduced by approximately 75%.
- CPM modulator/demodulator: The complexity is proportional to pM^L (where p is the number of phase states) but with $L = 3$ and a small modulation index set, it is comparable to a standard MSK demodulator and does not dominate the overall system burden [7,19].

4.6. Discussion and Comparative Summary

Table 3 provides a consolidated performance comparison. The proposed algorithm distinguishes itself by achieving significant PAPR suppression with no BER degradation through a non-distortive approach, maintaining high performance even in low-SNR and frequency-selective fading conditions. This makes it a robust and practical solution for next-generation satellite communications.

Table 3. Performance comparison with other PAPR suppression techniques.

Algorithm	PAPR Reduction	BER Performance	Computational Complexity
Proposed Polar-SLM-CPM	∼4.2 dB	No Degradation	Medium
Conventional SLM [10]	2.0–3.0 dB	No Degradation	High (V IFFTs)
Iterative PTS with Clipping [13]	2.6–3.2 dB	Slight Degradation	Very High
Weighted least squares SCR [14]	3.1–4.2 dB	Nearly No Degradation	Medium
Intelligent PAPR Suppression [13]	4.5–5.0 dB	Requires Training	High

Spectral Efficiency Trade-Off

The adoption of CPM introduces a controlled bandwidth expansion relative to the original OFDM signal. For a CPM signal with modulation index h and rectangular phase pulse of length L, the 99% power bandwidth B_{CPM} is approximately [24]:

$$B_{\text{CPM}} \approx 2\pi h \cdot \frac{1}{T} + \frac{2}{LT}. \tag{11}$$

In our system, h varies cyclically but averages $\bar{h} \approx 0.44$ and $L = 3$. Taking $T = T_s$, the normalized bandwidth $B_{\text{CPM}} T_s \approx 2\pi \cdot 0.44 + 2/3 \approx 3.43$, which is about 1.7 times the Nyquist bandwidth of the OFDM signal. However, the actual spectral efficiency of the COFDM-CPM waveform is degraded by only a factor of ∼1.5 compared to pure OFDM when considering the guard bands, thanks to the excellent spectral containment of the raised-cosine pulse. Moreover, the multi-index scheme is deliberately chosen to keep h small on average, thereby limiting the bandwidth expansion while preserving the constant-envelope benefit. In future designs, one can trade a slight increase in h for an even lower PAPR at the cost of reduced spectral efficiency; the PSO optimization can directly incorporate a spectral efficiency constraint into the fitness function.

5. Conclusions

This paper addresses the high PAPR problem in COFDM satellite communication systems by proposing a cooperative algorithm that combines polar coding, intelligent selective mapping, and continuous phase modulation. Theoretical analysis and MATLAB simulations confirm that the algorithm achieves approximately 4.2 dB PAPR reduction at $\text{CCDF} = 10^{-3}$ compared to the original OFDM signal, without introducing any meaningful BER degradation. The integration of a gradient-learning-optimized intelligent SLM reduces the IFFT-related complexity by approximately 75% compared to a conventional SLM. Detailed analyses of synchronization, parameter sensitivity, spectral efficiency trade-offs, and robustness in nonlinear/phase-noise channels further validate the practicality of the proposed scheme. Future work will focus on hardware-in-the-loop validation with real satellite transponders and extension to MIMO-OFDM satellite architectures.

Author Contributions: Conceptualization, J.X. and Y.Z.; methodology, J.X. and M.W.; software, X.Z.; validation, J.X., M.W. and X.Z.; formal analysis, Y.Z.; investigation, J.X.; resources, J.X.; data curation, X.Z.; writing—original draft preparation, J.X.; writing—review and editing, M.W. and Y.Z.; visualization, X.Z.; supervision, Y.Z.; project administration, J.X.; funding acquisition, J.X. All authors have read and agreed to the published version of the manuscript.

Funding: This research was funded by the National Key Research and Development Program Project of China (Grant No. 2023YFF0615700) and the Open Research Fund of Anhui Province Key Laboratory of Machine Vision Inspection (KLMVI-2024-HIT-19).

Institutional Review Board Statement: Not applicable.

Informed Consent Statement: Not applicable.

Data Availability Statement: The simulation data presented in this study are available on request from the corresponding author due to ongoing research.

Acknowledgments: The authors thank the anonymous reviewers for their constructive comments.

Conflicts of Interest: Author Jinsong Xu was employed by the company Wuhu HIT Robot Technology Research Institute Co., Ltd. The remaining authors declare that the research was conducted in the absence of any commercial or financial relationships that could be construed as a potential conflict of interest.

Abbreviations

The following abbreviations are used in this manuscript:

PAPR	Peak-to-Average Power Ratio
OFDM	Orthogonal Frequency Division Multiplexing
COFDM	Coded Orthogonal Frequency Division Multiplexing
CPM	Continuous Phase Modulation
SLM	Selective Mapping
PTS	Partial Transmit Sequence
CCDF	Complementary Cumulative Distribution Function
BER	Bit Error Rate
AWGN	Additive White Gaussian Noise
SNR	Signal-to-Noise Ratio
IFFT	Inverse Fast Fourier Transform
FFT	Fast Fourier Transform
QAM	Quadrature Amplitude Modulation
PSO	Particle Swarm Optimization
SCL	Successive Cancellation List
LLR	Log-Likelihood Ratio
HPA	High-Power Amplifier

References

1. Yang, Y. Basic framework of resilient PNT. *Acta Geod. Cartogr. Sin.* **2018**, *47*, 893–897. (In Chinese)
2. Xue, L.; Wang, Z.; Liu, Y. Analysis of the U.S. Department of Defense Positioning, Navigation and Timing (PNT) Strategy Report. *Aerosp. Missile J.* **2020**, *2*, 82–89. (In Chinese)
3. Xi, H. U.S. Department of Homeland Security releases report on PNT backup capabilities. *GNSS World China* **2020**, *45*, 27. (In Chinese)
4. Cao, S.; Li, X.; Zhang, Y. Multi-slots joint MLE relative navigation algorithm based on INS/JTIDS/BA for datalink network. *IEEE Access* **2020**, *8*, 136795–136807. [CrossRef]
5. Prasad, K.N.R.S.V. *OFDM for Wireless Communications Systems*; Artech House: Norwood, MA, USA, 2004.
6. Tasadduq, I.A.; Rao, R.K. OFDM-CPM signals. *Electron. Lett.* **2002**, *38*, 80–81. [CrossRef]
7. Pasupathy, S. Minimum shift keying: A spectrally efficient modulation. *IEEE Commun. Mag.* **1979**, *17*, 14–22. [CrossRef]
8. Ai, G.; Mao, Y.; Li, X. Principle of positioning system based on communication satellite. *Sci. China Ser. G* **2008**, *38*, 1615–1633. [CrossRef]
9. Han, S.H.; Lee, J.H. An overview of peak-to-average power ratio reduction techniques for multicarrier transmission. *IEEE Wirel. Commun.* **2005**, *12*, 56–65.
10. Bäuml, R.W.; Fischer, R.F.H.; Huber, J.B. Reducing the peak-to-average power ratio of multicarrier modulation by selected mapping. *Electron. Lett.* **1996**, *32*, 2056–2057. [CrossRef]
11. Nivetha, V.; Sudha, V. Modified μ-law root companding for PAPR reduction in GFDM signals. *Phys. Commun.* **2023**, *57*, 102013.
12. Wan, Y.; Liu, X.; Li, Z. PAPR-degraded secure OFDM-WDM-PON based on chaotic set-partitioned SLM. *IEEE Photon. Technol. Lett.* **2021**, *33*, 1387–1390. [CrossRef]
13. Zhang, T.; Wang, Y.; Chen, L. A novel PAPR reduction scheme based on joint traditional algorithm and machine learning for CO-OFDM systems. *IEEE Photon. Technol. Lett.* **2023**, *35*, 418–421. [CrossRef]
14. Liu, Z.; Zhang, H.; Zhao, Q. Research on PAPR suppression of OFDM signals based on improved subcarrier reservation algorithm. *J. Electron. Inf. Technol.* **2024**, *46*, 1196–1202. (In Chinese)

15. Liu, Z.; Wang, X.; Zhang, Y. Low-complexity PAPR reduction method for OFDM systems based on real-valued neural networks. *IEEE Wirel. Commun. Lett.* **2020**, *9*, 1840–1844. [CrossRef]
16. Nguyen, T.; Lee, M.; Park, S. Optimization of partial transmit sequences for PAPR reduction of OFDM signals without side information. *IEEE Trans. Broadcast.* **2022**, *69*, 313–321. [CrossRef]
17. Liu, X.; Wang, H.; Zhou, Y. PAPR reduction using iterative clipping/filtering and DMM approaches for OFDM-based mixed-numerology systems. *IEEE Trans. Wirel. Commun.* **2020**, *19*, 2586–2600. [CrossRef]
18. Xing, Z.; Ma, Y.; Sun, L. Variation approach-based nonlinear companding scheme for PAPR reduction in OFDM systems. *IEEE Trans. Broadcast.* **2022**, *68*, 916–929. [CrossRef]
19. Viholainen, A.; Ihalainen, T.; Renfors, M. Analysis and implementation of polynomial-based interpolation filters for bandwidth-efficient multi-standard radios. *IEEE Trans. Circuits Syst. I Reg. Pap.* **2009**, *56*, 1624–1637.
20. Arikan, E. Channel polarization: A method for constructing capacity-achieving codes for symmetric binary-input memoryless channels. *IEEE Trans. Inf. Theory* **2009**, *55*, 3051–3073. [CrossRef]
21. Zhang, S.; Shahrava, B. A SLM scheme for PAPR reduction in polar coded OFDM-IM systems without using side information. *IEEE Trans. Broadcast.* **2021**, *67*, 463–472. [CrossRef]
22. 3GPP. *Study on New Radio (NR) Access Technology*; 3GPP TR 38.912; V16.0.0; 3GPP: Sophia Antipolis, France, 2018.
23. *ITU-R Recommendation P.618-13*; ITU-R, Propagation Data and Prediction Methods Required for the Design of Earth-Space Telecommunication Systems. ITU-R: Geneva, Switzerland, 2017.
24. Proakis, J.G.; Salehi, M. *Digital Communications*, 5th ed.; McGraw-Hill: New York, NY, USA, 2008.